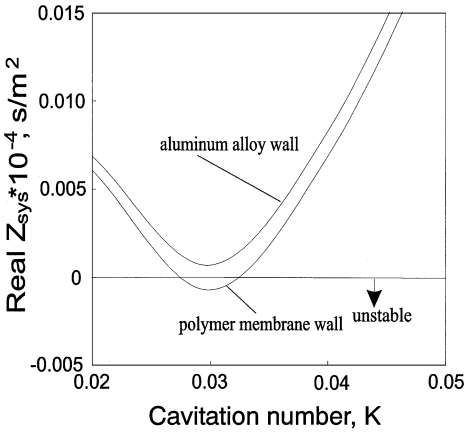


**Fig. 3 Stability margin: effect of tank flexibility.**

Young's modulus elasticity of the tank wall material of the outer tank, respectively.

Figure 3 presents the propulsion system stability curves for membrane and aluminum alloy materials for inner tank wall. In these computations, the feedline length was 2.2 m, and the feedline pressure drop $\Delta\bar{p}$ was 0.04 MPa. For the propulsion system with the wall thickness of the membrane tank of 0.0015 m, taking into account the effective bulk modulus $E_e$ led to a decrease in the effective acoustic speed $C_{\text{eqo}}$ for the oxidizer tank up to 50 m/s and made the propulsion system unstable at cavitation number $K = 0.03$ (Fig. 3). A decrease in the wall thickness of the inner membrane tank and in $E_e$ lowers the effective acoustic speed and reduces the stability margin of the system. In this numerical example, Young's modulus of the membrane is assumed to be one-seventh of that of aluminum alloy and the thickness one-fourth. In general, the thickness of a metal inner tank is determined not only by the differential pressure but also by the buckling load and/or sloshing load. On the other hand, the thickness of the membrane tank can be thinner because a membrane material is tolerant to small wrinkling and bending deformation. Therefore, the difference of the stability region in Fig. 3 for membrane and metal can be larger for the actual case.

## Conclusions

Rocket propulsion systems with a concentric tank structure are potentially unstable with respect to self-excited fluid oscillations caused by the pump cavitation phenomenon when short feedlines are used, as shown for a launch vehicle with a membrane-type tank and the studied rocket engine. Increasing compliance of the walls of the inner membrane tank reduces the system stability margins. A developed approach allows for a consistent and accurate prediction of the propulsion system stability without a preliminary experimental study of system elements, and the approach points to ways to eliminate the propulsion system instability. Methods for stabilization of such systems should be based on a correction of the dynamic properties of the feedlines and engine pumps.

## References

[1]Mankins, J. C., "Lower Costs for Highly Reusable Space Vehicles," *Aerospace America*, March 1998, pp. 36–42.

[2]Sutton, G. P., *Rocket Propulsion Elements: An Introduction to the Engineering of Rockets*, 6th ed., Wiley, New York, 1992, Chap. 7.

[3]Komatsu, K., Sano, M., Kasai, T., Ikawa, H., Kimura, J., Yamamoto, M., and Ohyagi, T., "Concept Study of Membrane Tank for Spacecraft," AIAA 2000-1572, 41st Structures, Structural Dynamics, and Materials Conference, Atlanta, April 2000.

[4]Pilipenko, V. V., Zadontsev, V. A., and Natanzon, M. S., *Cavitational Self-Excited Oscillations and Dynamics of Hydraulic Systems*, Mashinostroyenie, Moscow, 1977, pp. 198–220 (in Russian).

[5]Pilipenko, V. V., "Providing the LPRE—Rocket Structure Dynamic Compatibility," AIAA 93-2422, 29th Joint Propulsion Conference and Exhibit, Monterey, CA, June 1993.

[6]Shimura, T., "Geometry Effects in the Dynamic Response of Cavitating LE-7 Liquid Oxygen Pump," *Journal of Propulsion and Power*, Vol. 11, No. 2, 1995, pp. 330–336.

[7]Oppenheim, B. W., and Rubin, S., "Advanced Pogo Stability Analysis for Liquid Rockets," *Journal of Spacecraft and Rockets*, Vol. 30, No. 3, 1993, pp. 360–373.

[8]Nakajima, M., Mizohata, K., and Sawada, K., "Conceptual Design of the LE-7-Based Reusable Launch Systems," AIAA 98-0304, 36th AIAA Aerospace Sciences Meeting and Exhibit, Reno, NV, Jan. 1998.

# Experimental Evaluation of Mass Capture Ratio of Scramjet Inlets

Takeshi Kanda,* Tetsuo Hiraiwa,† Muneo Izumikawa,‡ and Tohru Mitani*

*National Aerospace Laboratory of Japan, Miyagi 981-1525, Japan*

## Introduction

SCRAMJET engine models 2 m in length have been tested at the Ramjet Engine Test Facility (RJTF) of the National Aerospace Laboratory of Japan.[1] The captured-air-mass flow rates of the models are necessary for estimating the equivalence ratios and combustion efficiencies. However, the high cost associated with operating the RJTF limits the number of mass flow measurement tests conducted. Thus, the authors measured mass-capture ratios in a pilot wind tunnel (PWT), which is smaller than the RJTF, and then estimated the ratios of the RJTF engine models. An empirical equation for the ratio of sidewall-compression-type inlet models was constructed, which clarified effects of the inflow conditions and the inlet configurations on the ratio empirically.

## Experimental Apparatus

Figure 1 shows a schematic diagram of the PWT and the equipment used to measure the mass capture of an inlet model. This equipment was similar to the previous ones used to measure the mass-capture ratio.[2] This tunnel can supply airflow at Mach 3.4, 5.3, and 6.7. The nozzles of the PWT were 1/5 as large of those of the RJTF and each had an exit area of $100 \times 100$ mm. There was a choked valve far downstream of the inlet diffuser. The air was heated to 700 K in Mach 5.3 and 6.7 tests but was not heated in Mach 3.4 tests. The total pressure of the airflow was 6 MPa.

In most of the tests, the level of the inner surface of the nozzle was the same as that of the top wall surface of the inlets. In some tests, however, the inlets were set in the freestream and the inviscid part of the air flowed into the inlet models, whereas the boundary layer from the PWT flowed out of the models. Table 1 lists the test conditions. When the gap between the top wall of the model and the wind-tunnel nozzle wall was 30 mm, the model was in the freestream. When the gap was 8 mm, part of the boundary layer flowed into the inlet. A 1/7 power-law profile of the velocity and a Crocco–Busemann relation

Presented as Paper 2003-0011 at the Aerospace Sciences Meeting and Exhibit, Reno, NV, 6 January 2003; received 1 May 2003; revision received 21 October 2003; accepted for publication 2 November 2003. 

*Leader, Ramjet Propulsion Research Center, Kakuda. Senior Member AIAA.

†Senior Researcher, Ramjet Propulsion Research Center, Kakuda. Member AIAA.

‡Senior Researcher, Ramjet Propulsion Research Center, Kakuda.

**Table 1 Mass-capture ratio of the inlet models measured in the pilot wind tunnel and the corresponding mass-capture ratio in the RJTF tests**

| | Inlet configuration | | | | | | |
|---|---|---|---|---|---|---|---|
| Variable | No strut | No strut | Strut A | No strut | Strut A | Strut B | Strut A + ramp |
| | $M3.4$[a] | $M5.3$ | $M5.3$ | $M6.7$ | $M6.7$ | $M6.7$ | $M6.7$ |
| Gap between model top wall and wind-tunnel wall | 0 | 0 | 0 | 0 | 8 mm | 8 mm | 30 mm |
| Contraction ratio | 2.9 | 2.9 | 5.0 | 2.9 | 5.0 | 8.3 | 9.3 |
| Pilot wind-tunnel capture ratio | 0.72 | 0.87 | 0.83 | 0.91 | 0.87 | 0.76 | 0.84 |
| | $M4$[b] | $M6$ | $M6$ | $M8$ | $M8$ | $M8$ | $M8$ |
| RJTF capture ratio | 0.72 | 0.87 | 0.83 | 0.91 | 0.86 | 0.74 | 0.81 |

[a]Pilot wind-tunnel test condition. [b]RJTF test condition.

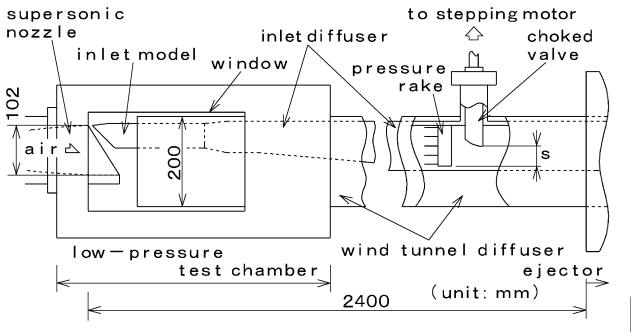


**Fig. 1 Pilot wind tunnel and equipment for mass-capture measurement.**

for the temperature profile in the boundary layer were adopted to estimate the displacement thickness.

First, the choked valve was open and the airflow was supersonic throughout the inlet and the diffuser. As the valve was moved down, the airflow in the inlet diffuser finally became subsonic and choked at the valve. The discharge coefficient was calibrated with a choked venturi nozzle with a diameter of 40 mm. The geometry of the nozzle was according to ISO specifications.[3]

Figure 2 shows three inlet models and Table 1 lists the configurations of these models. The size of these was 1/5 that of the scramjet models tested in the RJTF, except for the standard mass-capture model.

Mass flow rate, $\dot{m}$, is expressed as follows under conditions of choking:

$$\dot{m} = A_v P_{tv} \sqrt{\frac{\gamma}{RT_{tv}}} \frac{1}{[(\gamma+1)/2]^{(\gamma+1)/2(\gamma-1)}} \tag{1}$$

$A_v$ is the cross section of the choked valve. $P_{tv}$ and $T_{tv}$ are total pressure and total temperature, respectively, measured ahead of the valve; $T_{tv}$ was measured with a single thermocouple; $\gamma$ is the ratio of the specific heats; and $R$ is the gas constant of air. In Mach 6.7 tests, the standard mass-capture model was used (Fig. 2). This model had no spillage. At the same valve opening, the mass-capture ratio $\eta_{\text{cap}}$ was determined by comparing the total pressure of the inlet models with that of the standard capture model:

$$\eta_{\text{cap}} = \frac{(P_{tv}/P_t)}{(P_{tv}/P_t)_{\text{ref}}} \sqrt{\frac{(T_{tv}/T_t)_{\text{ref}}}{(T_{tv}/T_t)}} \tag{2}$$

Here, ref represents the reference condition of the standard mass-capture model. $P_t$ and $T_t$ are total pressure and total temperature in the reservoir, respectively.

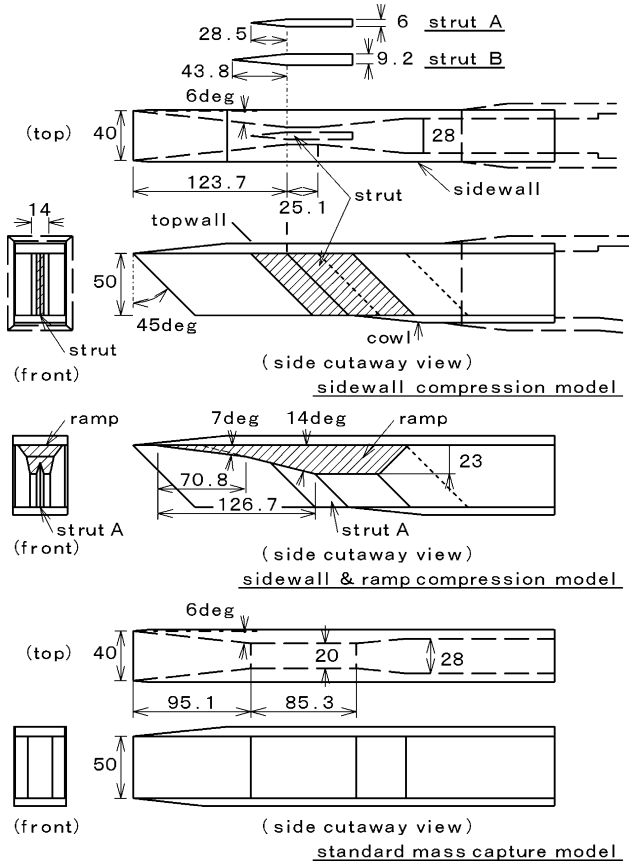


**Fig. 2 Inlet models.**

## Results and Discussion

### Mass-Capture Ratio

The measured mass-capture ratios are listed in Table 1. The error was ±0.02. The ratios of the RJTF models were estimated based on these results from the PWT tests. The test conditions with entrance Mach numbers of 3.4, 5.3, and 6.7 correspond to flight conditions of Mach 4, 6, and 8, respectively, at the RJTF. These flight conditions are also listed in Table 1.

### Empirical Equation for Mass Capture Ratio

Masuya and Wakamatsu correlated the experimental results of the capture ratio $\eta_{\text{cap}}$ with an inflow Mach number, $M$ (Ref. 4):

$$\eta_{\text{cap}} = 0.96[1 - 3.5 \times \exp(-0.75M)] \tag{3}$$

This equation predicts the effect of the Mach number with reasonable accuracy. However, there were no factors for the model geometrical features and the incoming boundary-layer condition. The authors modified the equation to include such parameters, using the results in the PWT and data in the literature.[5–8] The following parameters were selected:

1) Effective inlet height $h_e$, as found by subtracting the displacement thickness from the geometrical height $h$ is formatted to $(h_e/h)^{n1}$. As the inflow boundary layer becomes thick, the secondary flow area increases.

2) Length from the inlet entrance to the cowl leading edge $L$ is formatted to $(h_e/L)^{n2}$. The mass-capture ratio increases as the cowl covers the bottom area ahead of it.

3) Length of a strut $l$ is formatted to $\{(L-l)/L\}^{n3}$. The strut induces the boundary layer, and the ridgeline at the bottom plane increases with attachment of the strut.

4) Swept angle of the sidewall $SW$ in degrees, is formatted to $\{(90–SW)/SW\}^{n4}$. As the swept angle increases, the velocity component parallel to the leading edge increases.

5) The contraction ratio $CR$ is formatted to $(1/CR)^{n5}$. The mass-capture ratio decreases as the number of reflections of the shock

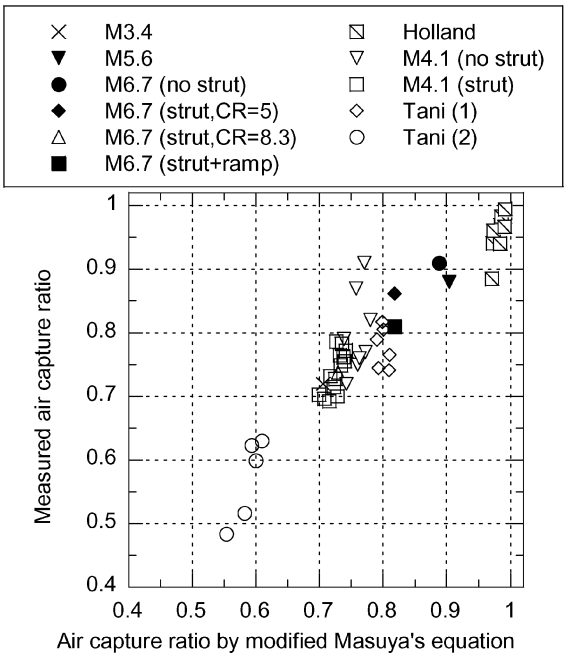


**Fig. 3 Mass-capture ratio predicted by modified Masuya equation.**

waves increases. The number increases with increasing contraction ratio.

In the data, $h_e$ was from 80 to 100% of $h$; $L$ was from 0% to 50% of the length from the inlet entrance to the throat; $l$ was from 9% to 27% of the inlet length; $SW$ was from 30 to 60 deg; and $CR$ was from 2.9 to 9.3. Width at the entrance was not selected as a parameter because the widths of the inlets adopted here were in a narrow range, from 0.8 to 1 of the inlet height.

The modified mass-capture ratio $\eta_{\text{cap},m}$ was expressed using the modification factor $f$ and the parameters $n1 = 10$, $n2 = 0.4$, $n3 = 1$, $n4 = 0.1$, and $n5 = 0.5$:

$$\eta_{\text{cap},m} = (\eta_{\text{cap}}\,[\text{by Masuya's equation}]) \times f(x) \tag{4}$$

$$x = \left(\frac{h_e}{h}\right)^{10}\left(\frac{h_e}{L}\right)^{0.4}\left(\frac{L-\ell}{L}\right)\left(\frac{90-SW}{90}\right)^{0.1}\left(\frac{1}{CR}\right)^{0.5} \tag{5}$$

The modification factor was attained empirically from the data of the mass-capture ratios:

$$f = -0.0092/x + 1.05 \tag{6}$$

Figure 3 shows the correlation between the test data and the calculated capture ratio by Masuya's equation. Correlation between the experimental values and the calculated values was 0.94.

Equation (5) shows that the effect of the boundary layer on the capture ratio was large. The inflow boundary layer should be thin. The effect of the strut was also large. Neither the effect of the swept angle nor the length of the inlet affected the mass-capture ratio greatly.

## Conclusions

Air-mass capture ratios of the scramjet inlet models were measured in the PWT at Mach 3.4, 5.3, and 6.7 conditions. The ratios of the RJTF test models were estimated with the test data from the PWT. An empirical equation was constructed for the mass-capture ratio of the sidewall-compression-type inlets. The equation showed that the effect of the boundary layer and the effect of the strut were large.

## References

[1]Chinzei, N., "Research Activities on Scramjets at NAL-KRC in Japan," 15th International Symposium on Air Breathing Engines, ISABE 2001-1075, Sept. 2001.

[2]Hudgens, J. A., and Trexler, C. A., "Operating Characteristics at Mach 4 of an Inlet Having Forward-Swept, Sidewall-Compression Surfaces," AIAA Paper 92-3101, July 1992.

[3]"Measurement of Gas Flow by Means of Critical Flow Venturi Nozzles," ISO9300, 1990.

[4]Masuya, G., and Wakamatsu, Y., "Calculation of Scramjet Performance," National Aerospace Lab., NAL TR-987, Tokyo, Japan, July 1988 (in Japanese).

[5]Holland, S. D., "Computational Parametric Study of Sidewall-Compression Scramjet Inlet Performance at Mach 10," NASA TM 4411, Feb. 1993.

[6]Kanda, T., Komuro, T., Masuya, G., Kudo, K., Murakami, A., Tani, K., Wakamatsu, Y., and Chinzei, N., "Mach 4 Testing of Scramjet Inlet Models," *Journal of Propulsion and Power*, Vol. 7, No. 2, 1991, pp. 275–280.

[7]Tani, K., Kanda, T., Kudou, K., Murakami, A., Komuro, T., and Ito, K., "Aerodynamic Performance of Scramjet Inlet Models with a Single Strut," AIAA Paper 93-0741, Jan. 1993.

[8]Tani, K., Kanda, T., and Tokunaga, T., "Starting Characteristics of Scramjet Inlets," *Proceedings of 11th International Symposium on Air-Breathing Engines*, Vol. 1, AIAA, Washington, DC, 1993, pp. 1071–1080.

# Nucleation Mechanism for Freezing of Alumina in Solid Propellant Rocket Motor Nozzles

Daniel E. Rosner*
*Yale University, New Haven, Connecticut 06520-8286*

## I. Introduction, Background, Objectives

IT is well known that the addition of appreciable amounts of aluminum powder (e.g., ca. 15–20 wt.%) to conventional double-base solid propellants can improve their performance (e.g., specific impulse, etc.).[1] However, the achievable performance gain will certainly depend upon the location of the release of the heat of molten alumina crystallization during the droplet-laden gas expansion process.[2] Moreover, the location of alumina freezing will also dramatically influence the optical properties of such plumes.[3,4] Until now, there has evidently been no simple method to estimate the spatial location and distribution of the volumetric rate of release of this appreciable latent heat. While undercoolings of as much as around 20% of the equilibrium freezing point[5,6] are known to be possible in principle, actual performance experience indicates that such extreme delayed freezing probably does not occur, at least for the bulk of the alumina present. In this Note we propose a plausible explanation for this, and one which, with further development, promises to enable rational predictions of crystallization rates in metallized solid-(propellant)-rocket-motor (SRM) combustion products.

## II. Theory of Alumina Nanodroplet Freezing

Using typical numbers for aluminized SRM situations [e.g., the space shuttle solid rocket boosters (SRBs); compare Table 1], we

Received 23 September 2003; accepted for publication 28 October 2003.


*Professor, Center for Combustion Studies, Chemical and Mechanical Engineering, and Engineering Consultant, Mason Laboratory, 9 Hillhouse Avenue; daniel.rosner@yale.edu.